MRS Advances © 2019 Materials Research Society. This is an Open Access article, distributed under the terms of the Creative Commons Attribution licence (http://creativecommons.org/licenses/by/4.0/), which permits unrestricted re-use, distribution, and reproduction in any medium, provided the original work is properly cited.
DOI: 10.1557/adv.2019.255

The Discharge Mechanism for Solid-State Lithium-Sulfur Batteries

Erika Nagai[1,2], Timothy S. Arthur*[1], Patrick Bonnick[1], Koji Suto[1] and John Muldoon[1]

[1]*Toyota Research Institute of North America, 1555 Woodridge Avenue, Ann Arbor, MI 48105, USA*

[2]*Toyota Motor Corporation, Higashifuji Technical Center, 1200 Mishuku, Susono, Shizuoka 410-1193, Japan*

**Corresponding author: Timothy S. Arthur (tim.arthur@toyota.com)*

Abstract

The electrochemical discharge mechanism is reported for all-solid lithium sulfur batteries. Upon milling with carbon fibers, the solid electrolyte used within the cathode composite becomes electrochemically active. Analysis with Raman spectroscopy and XPS revealed the importance of bridging S-S bond formation and breaking in lithium polysulfidophosphates during electrochemical lithiation of the active solid electrolyte. Remarkably, when sulfur is introduced as an active material in the cathode composite, lithium polysulfides are formed as an intermediate product before full lithiation into lithium sulfide. The synthesis of materials based on bridging S-S bonds is an important avenue to the design of new cathodes for all-solid batteries.

INTRODUCTION:

To power the future of mobility, diverse energy storage systems are critical as society moves towards electric, hybrid and fuel-cell powered vehicles. Vehicle electrification carries additional complexities of safety, range and cost to achieve

practical product development. Li-ion batteries have emerged as a leading candidate to replace Ni-MH batteries, however, the need for longer-lasting, faster-charging, further-range electric vehicles has diversified research into *post*-Li-ion battery materials, structure and systems [1-3]. One potential, attractive replacement is solid-state batteries; which premise is to replace the organic liquid electrolytes typically found in Li-ion batteries with a solid-state ion conductor [4,5]. Wide electrochemical windows, non-flammability, and the potential to realize the lithium metal anode are advantages pushing solid-state batteries to the fore-front of the next generation of energy storage. However, to compete with conventional, liquid electrolytes, achieving high Li^+ conductivity is a tremendous challenge.

The field of solid-state ionics has progressed rapidly, and the variety of Li-ion conductors which can realize fast Li^+ transport at moderate temperatures are enabling the next generation of electrochemical storage. Polymer, gel, molten salt and ceramic electrolytes have strengths and challenges when faced with integration into practical devices; however, sulfide-based electrolytes have emerged as contender whose conductivity can match, and surpass, organic-liquid electrolytes [6]. LGPS, $Li_7P_3S_{11}$ glass-ceramic, argyrodite $Li_{9.54}Si_{1.74}P_{1.44}Cl_{0.3}$ are examples of electrolytes which have shown excellent Li^+ conductivity, albeit with mixed results on the electrochemical window and the ability to withstand the strong reductive potential of Li-metal[5,7-9]. Sakamoto *et al.*[10] have evidenced the reductive formation of Li_2S and Li_3P products from lithium thiophosphate, Li_3PS_4, after cycling with symmetric Li-Li cells via Raman spectroscopy, which have been confirmed by *in situ* XPS experiments and predicted via DFT calculations [11,12]. Sulfide electrolytes have also been shown to react with high-voltage cathode, and the formation of a thin-interface is sufficient to deteriorate the battery capacity and cycling capabilities. To enable the technology, surface modification with $LiNbO_3$ serves to hinder the chemical cross-diffusion and reduce the lithium depletion at the space-charge layer [13]. Research into high-energy cathodes is pivotal to realizing all-solid lithium batteries.

The emergence of sulfur as a high-energy density cathode is the product of cathode, electrolyte and separator technology aimed at accomplishing reversible capacity at high rates. The merits of sulfur are the high theoretical capacity (1675 mAh g^{-1}), which balances the low average cathode discharge potential (~2.0 V) to yield a high theoretical energy density (~2600 Wh kg^{-1}). However, significant challenges must be overcome, such as the dissolution of sulfur and polysulfides into the electrolyte, the continual decomposition of the organic electrolyte, and dendritic growth of lithium metal. The result is the inability to retain capacity over extended cycling, and the solution has manifested as elegant materials design and engineering to encapsulate and protect the active material. Carbon, polymer and separator technology have all played vital roles in realizing the high-loading and sustainable sulfur cathodes [14-16]. Alternatively, replacement of the organic, liquid electrolyte may provide a multi-faceted route to solve continuous SEI formation and polysulfide dissolution, thus solid-state Li-S batteries have the potential to have excellent cycle-life. Indeed, utilizing solid-electrolytes have shown improved capacity retention without encapsulation of the active materials, which paves the way for high-loading of the active materials for increased energy density at a potentially lower cost [17-20]. To make such an improvement, an elucidation of the discharge mechanism will deepen the understanding of the electrochemical reactions, and provide insights to further improve the design and processes needed to scale-up the battery electrodes.

Here, we investigate how the process of making composite cathodes for solid-state sulfur cathodes impacts the electrochemical discharge by separating the reactivity of the three essential components: carbon, solid-state electrolyte (amorphous-Li_3PS_4, LPS), and sulfur/lithium sulfide. Researchers have recently realized the

electrochemical activity of lithium thiophosphate electrolytes [21,22], and here we demonstrate the impact of that activity on the AS-LiS battery discharge mechanism.

EXPERIMENTAL

Chemical Synthesis: Li_3PS_4 (LPS) was synthesized through mechanical milling of Li_2S and P_2S_5 (Aldrich) in a 3:1 molar ratio. The milling was performed on a 2g scale. The milling was performed in ZrO_2 pot (45 ml) and 32 g of 5 mm diameter ZrO_2 balls. Milling is performed at 320 RPM for 30 hs.

Cathode composites: (A) Sulfur/Carbon Fibers (Aldrich)/SE composite: Sulfur : CF : Li_3PS_4 are combined in a 35.9 : 20.5 : 43.6 mass ratio and mixed with motor and pestle. Then 1g of the mixture was added to a 45 ml ZrO_2 jar with 32 g of 5mm (dia) ZrO_2 balls. The mixture was milled at 500 RPM for 20 h to form the composite. (B) CF:Li_3PS_4 was combined in a 20.5 : 43.6 mass ratio and mixed with a motor and pestle. Then 1g of the mixture was added to a 45 ml ZrO_2 jar with 32 g of 5mm (dia) ZrO_2 balls. The mixture was milled at 500 RPM for 20 h to form the composite.

Electrochemical Analysis: ~0.2 g of the solid electrolyte, LPS, was pressed at 4 tons/cm2 to form the separator layer. Then the cathode composite, (A) or (B), was added to one side and pressed at 3 ton cm^{-2}. Mechanically polished lithium foil was added to the opposite side to act as an anode. The cell-stack was held at 2 $N{\cdot}m^2$ pressure.

X-ray Photoelectron Spectroscopy: XPS analysis was performed on cathode composites after dismantling the cell. Samples were transferred under an inert atmosphere. Peak-fitting analysis was performed in the Multipak analysis software. Spectra were collected with a Al $K\alpha_{1,2}$ (1486.6 eV) source with a pass energy of 29.35 eV. The S2p peak was fit after background subtraction (Shirley) and a 2p3/2:2p1/2 ratio of 2:1. All spectra are aligned to adventitious carbon at C1s = 284.7 eV. Quantification is performed using peak intensities and instrument sensitivity factors.

Raman: Raman analysis was performed on cathode composites after dismantling the cell. Samples were transferred under an inert atmosphere.

RESULTS AND DISCUSSION

Electrochemical Discharge of the Sulfur, Carbon Fiber, and LPS Electrode

Figure 1 is the 1st and 2nd discharge of an all-solid lithium-sulfur battery from at a slow C/30 rate. On the second cycle, we observe an increase in open-circuit potential (OCP), 2.16 V→ 2.35 V, and improved capacity, 2.6 mAh → 3.4 mAh, respectively. As a note, the theoretical capacity of this cathode is 4.2 mAh. First as compared to the galvanic discharge of a similar sulfur cathode, the shape of the potential curve indicates a different reaction mechanism than seen in liquid electrolytes [14]. Based on the shape of the second discharge, we defined three potential-limited regions of reaction; a high-potential reaction region is observed at the beginning of discharge (2.35 V → 2.20 V), a mid-potential reaction region (2.20 V → 2.06 V), and a 2 V-plateau region (2.06 V → 1.5 V). The cathode composite is extracted after galvanic reduction to the labeled State-of-Charge (SOC) or Depth-of-Discharge (DOD), and analyzed with X-ray Photoelectron Spectroscopy (XPS) and Raman without exposure to ambient air.

Fortunately, there is a wealth of reference information to fingerprint known materials and assign the bonding of the possible sulfide species in the composite cathode [23-26].

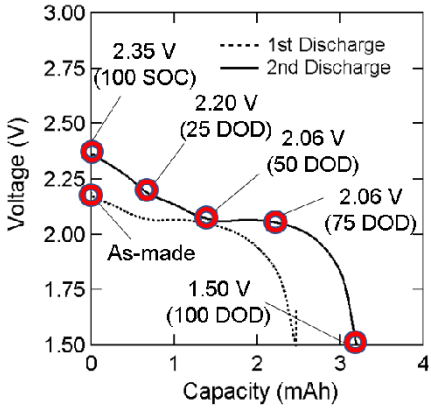

Although the active material sulfur, S_8, is stable in air, sulfide-based electrolytes are known to decompose upon exposure to air [27,28]. By understanding the state of the cathode under electrochemical discharge in all-solid Li-S batteries, we can design paths to increasing the active material utilization, rate and capacity.

Figure 1. 1st and 2nd galvanic discharge of a S:CF:LPS cathode composite. Points for Raman and XPS analysis are labelled.

Formation of Active $Li_3PS_4(\mu\text{-}S_x)S_4PLi_3$ ($x \geq 1$)

To ensure good mixing and solid-solid contact, the components of the cathode undergo rigorous milling to form the composite. Even without the presence of elemental sulfur (S_8), the composite made from a 6.2:1 (mol:mol) carbon fibers (CF):LPS is electrochemically active with an OCP = 1.68V and an initial discharge capacity of 1.2 mAh (Figure 2a). To investigate the role of carbon, carbon fibers (CF):LPS composites are synthesized in a (mol:mol) 1:0, 1:9, 3:7, 7:3, 9:1 and 1:0 ratios, and only composites formed from the 7:3 → 9:1 ratio are electrochemically active, with the 7:3 ratio showing the highest discharge capacity of 2.0 mAh. Under these conditions, the capacity increases with increasing LPS content, indicating that LPS is the electrochemically active component in the CF:LPS composites. Figure 2b) shows the Raman spectra of a CF:LPS composite (6.2:1), and a broad signal ranging from 380-405 cm^{-1} is evidence for the formation of $(P_2S_6)^{4-}$ and $(P_2S_7)^{4-}$ anions from the $(PS_4)^{3-}$ tetrahedra [29]. The formation of these anionic groups must be counter-balanced with a release of sulfur. In the C:LPS composites, we are not able to observe all the vibrational stretches to indicate S_8 formation. Interestingly, a broad peak centered at 480 cm^{-1} in the Raman spectrum clearly shows evidence for E_3 bonding signature of S-S bonds, which we assign to the formation of $(PS_{4+n})^{3-}$ anions, similar to the lithium polysulfidophosphates observed by Liang *et al.*[24]. However, as polysulfidophosphates have only previously been observed through a THF-based solution synthesis, the formation of the sulfur-bridged $(PS_4)^{3-}$ units is confirmed with S2p and P2p XPS, as shown in Figure 2c) and d), respectively. Although there is a shift to lower binding energies for the P2p signal in the bridged- anions, distinguishing the presence of bridged-S (green) from terminal-S (orange) is more clearly shown by a S2p peak at 163.5 eV, here use as an indicator of bridging sulfur [25]. Indeed, only the composites made within the active composition

range 7:3 → 9:1 show the characteristic new peaks in the XPS HRES spectra. We hypothesize that $Li_3PS_4(\mu\text{-}S_x)S_4PLi_3$ ($x \geq 1$) is the electrochemically active material when cycled with in a full-cell configuration.

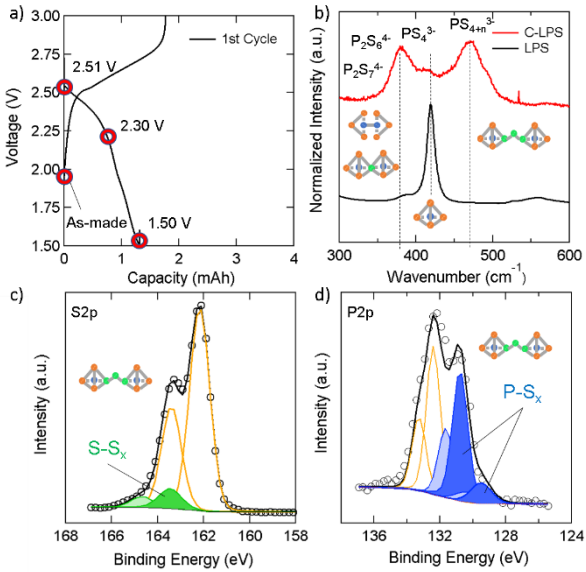

Figure 2a) Galvanic discharge, b) Raman spectrum, XPS c) S2p and d) P2p of a 6.2:1 CF:LPS (mol:mol) cathode composite.

Discharge Mechanism of CF:Li_3PS_4

Figure 3 shows the S2p spectra of the As-made composite, after the 1st charge, and limited to selected voltages labeled 1-3: 2.5 V, 2.2 V and 1.5 V, respectively. During oxidation of the cathode, the peak XPS S2p indicative of bridging S-S bonds at 163.5 eV increase in intensity relative to the terminal sulfides at 162.0 eV. Therefore, S-S bonds are formed during the electrochemical de-lithiation of the cathode composite layer. Conversely, the same bonds are broken as the cathode is discharged and lithiated, as the intensity of the bridging sulfur S2p peak decreases and the $(PS_4)^{3-}$ tetrahedra are restored. The electrochemical mechanism of the CF:LPS composites echoes the results of Tatsumisago *et al*. [22], where LPS and acetylene black composites were shown to be electrochemically active. The formation and breaking of linear S-S bonds is essential to understanding the mechanism of sulfur in solid-state composite cathodes.

Discharge Mechanism of S:CF:Li_3PS_4

The previous results indicates the presence of two active materials in the S:CF:LPS composites; the lithiated form of the CF:LPS composite and the un-lithiated S_8 active material. Therefore, the OCP of the As-made composite is mixed-potential of a discharged and charged cathode active materials. Consequently, the cathode was cycled galvanically for 1 cycle to electrochemically delithiate the entire cathode composite before the second discharge; therefore, the mechanism begins from a full state-of-charge

(100 SOC). Figure 4a) and b) show the Raman and XPS S2p results, respectively, as the composite cathode is discharge through the high- and mid-potential regions.

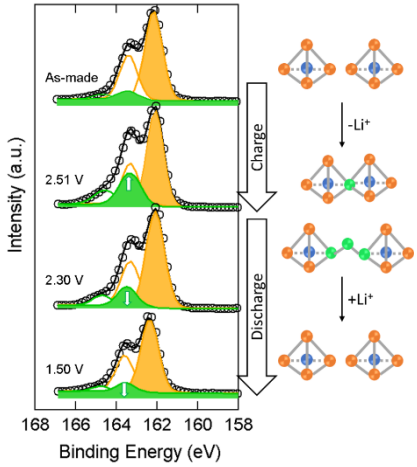

Figure 3. XPS S2p of a CF:LPS composite cathodes discharged to different depths-of-discharge (DOD).

In the Raman spectra, we identified these peaks as lithium polysulfide Li_2S_n ($n \geq 2$) and the active form of the LPS, $Li_3PS_4(\mu\text{-}S_x)S_4PLi_3$. Here, we designate the peak to $(PS_{4+n})^{3-}$ ($n \geq 1$), and observe decrease in intensity as the cathode is discharged from 100 SOC to 25 DOD. From the XPS data, the S2p peak representative of bridging sulfur decreases in intensity which confirms the cleaving of the bridging S-S bonds is responsible for the high potential discharge capacity. Therefore, the electrochemical activity within these potentials is the lithiation of the active LPS. As shown in Figure 4 in the mid-potential region, the sulfur ring, S_8, peak intensity decreases in both the Raman and XPS spectra. In addition, the S2p peak at 163.5 eV grows in intensity, which is counter-intuitive to the response seen for the lithiation mechanism of $Li_3PS_4(\mu\text{-}S_x)S_4PLi_3$.

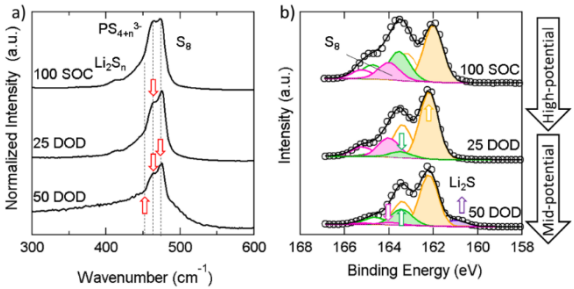

Figure 4. a) Raman and b) XPS S2p of a S:CF:LPS composite cathodes discharged from 100 SOC → 50 DOD.

Indeed, the intensity for PS_{4+n}^{3-} peak in the Raman spectra deceases in the Raman spectroscopy, as the shoulder for lithium polysulfides (Li_2S_n, 451 cm^{-1}) increases, thus revealing that the increase in the peak intensity for bridging S-S bonds in the S2p is the

formation of *lithium polysulfides* from S_8. Lithium polysulfide formation is well known in liquid-based sulfur cathodes, however, the formation of linear S-S bond structures also plays a key role in the solid-state. The analysis shows that lithium polysulfides are necessary in the discharge mechanism of sulfur in the solid-state.

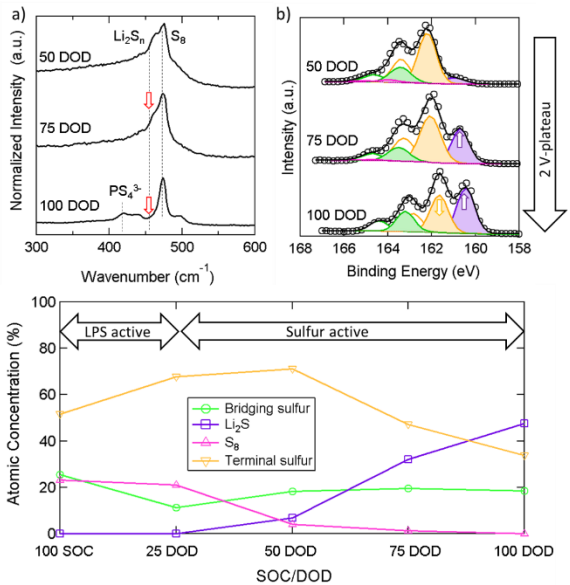

Figure 5. a) Raman and b) XPS S2p of a S:CF:LPS composite cathodes discharged from 50 DOD → 100 DOD. c) XPS quantification of S2p peaks S2p of a S:CF:LPS composite cathodes.

Finally shown in the Figure 5a) Raman analysis of the 2 V-plateau (50 DOD → 100 DOD), the LiS_n shoulder decreases in intensity concurrent to the growth in the Li_2S peak in the XPS S2p (Figure 5b). Lithium polysufides are transformed into the fully-lithiated Li_2S. Due to the strong ionic bond, the S2p XPS shows a clear growth of the peak at 160.7 eV representing Li_2S, a key discharge product whose intensity is often difficult to detect with Raman. Figure 5c) shows the atomic % of sulfur species present at different depths-of-discharge calculated from the peak-fitting analysis. Considering, that the capacity of the cathode is 3.4 mAh (1353 mAh/g_{sulfur}), the figure shows that from 100 SOC to 25 DOD of the S:CF:LPS composite, the first 0.85 mAh worth of charge is due to the the lithiation of the active LPS. Therefore, LPS accounts for ~0.85 mAh or ~25 % of the contribution to the total capacity. Importantly, Figure 5c) only quantifies the surface of the cathode and unreacted sulfur was detected within the cathode by Raman. Our analysis indicates that improving sulfur utilization is vital to maximizing the energy from all-solid lithium-sulfur cells.

CONCLUSION

In conclusion, the electrochemical discharge mechanism for all-solid Li-S batteries was determined to be combination of the intended sulfur active material, and the unintentional capacity gained from an active form of the solid-electrolyte. The formation and scission of linear S-S linkages are key to the electrochemical reaction with Li^+ ions,

and to achieve full utilization of the sulfur cathode requires improved cathode composite engineering. Also, metallic lithium dendrite penetration into the cathode must be stopped to analyze the cathode under extended cycling. Indeed, a deep investigation of the charging and cycling mechanisms will reveal the stability and capability of sulfur as a cathode for all-solid batteries.

ACKNOWLEDGMENTS

The authors would like to thank Tomoya Matsunaga, Masafumi Nose, Ximeng Li and Yukinari Kotani from Toyota Motor Corporation for their guidance and support of the research.

References:

1. M. Armand, and J.-M Tarascon, *Nature* **451**, 652 (2008).
2. M. Armand, and J.-M Tarascon, *Nature* **414**, 359 (2001).
3. B. Scrosati, J. Hassoun and Y.K.Sun, *Energy Environ. Sci.* **4**, 3287 (2011).
4. J.C. Backman, S. Muy, A. Grimaud, H.-H. Chang, N. Pour, S.F. Lux, O. Paschos, F. Maglia, S. Lupart, P. Lamp, L. Giordano and Y. Shao-Horn, *Chem. Rev.* **116**, 140 (2016).
5. N. Kamaya, K. Homma, Y. Yamakawa, M. Hirayama, R. Kanno, M. Yonemura, T. Kamiyama, Y. Kato, S. Hama, K. Kawamoto and A. Mitsui, *Nat. Mater.* **10**, 682 (2011).
6. Z. Zhang, Y. Shao, B. Lotsch, Y.-S. Hu, H. Li, J. Janek, L.F. Nazar, C.-W. Nan, J. Maier, M. Armand, and L. Chen, *Energy Environ. Sci.* **11**, 1945 (2018).
7. F. Mizuno, A. Hayashi, K. Tadanaga and M. Tatsumisago, *Adv. Mater*. **17**, 918 (2005).
8. Y. Kato, S. Hori, T. Saito, K. Suzuki, M. Hirayama, A. Mitsui, M. Yonemura, H. Iba and R. Kanno, *Nat. Energy*. **1**, 16030 (2016).
9. Y. Seino, T. Ota, K. Takada, A. Hayashi and M. Tatsumisago, *Energy Environ. Sci*. **7**, 627 (2014).
10. R. Garcia-Mendez, F. Mizuno, R. Zhang, T.S Arthur and J. Sakamoto, *Electrochim. Acta* **237**, 144 (2017).
11. S. Wenzel, D.A. Weber, T. Leichtweiss, M.R. Busche, J. Sann, and J. Janek, *Solid State Ionics* **286**, 24 (2016).
12. W. Richards, L.J. Miara, Y. Wang, J.C. Kim and G. Ceder, *Chem. Mater.* **28**, 266 (2016).
13. N. Ohta, K. Takada, L. Zhang, R. Ma, M Osada, and T. Sasaki, *Adv. Mater*.**18**, 2226 (2006).
14. A. Manthiram, S.-H. Chung and C. Zu, *Adv. Mater*. **27**, 1980 (2015).
15. Q. Pang, X. Liang, C.Y. Kwok and L.F. Nazar, *Nat. Energy* **1**, 16132 (2016).
16. P. Bonnick, E. Nagai and J. Muldoon, *J. Electrochem. Soc*.**165**, A6005 (2016).
17. S. Zhang, K. Ueno, K. Dokko, and K. Watanabe, *Adv. Energy Mater*.**5**, 15001177 (2015).
18. M. Nagao, A. Hayashi, M. Tatsumisago, T. Ichinose, T. Ozaki, Y. Togawa, and S. Mori *J. Power Sources*. **274**, 471 (2015).
19. T. Hakari,A. Hayashi and M. Tatsumisago, *Adv. Sustainable Syst.*, **1**, 1700017 (2017).
20. X. Judez, H. Zhang, C. Li, G.G. Eshetu, Y. Zhang, J.A. González-Marcos, M. Armand, and L.M. Rodriguez-Martinez, *J. Phys. Chem. Lett.* **8**, 3473 (2017).
21. H. Nagata and Y. Chikusa, Y. *J. Power Sources*. **329**, 268 (2016).
22. T. Hakari, M. Deguchi, K. Mitsuhara, T. Ohta, K. Saito, Y. Orisaka, Y. Uchimoto, Y.Kowada, A. Hayashi and M. Tatsumisago, *Chem. Mater*.**29**, 4768 (2017).
23. M. Hagen, P. Schiffels, M. Hammer, S. Dörfler, J. Tübke, M.J. Hoffmann, H. Althues, and S. Kaskel, *J. Electrochem. Soc.* **160**, A1205 (2013).
24. Z. Lin, Z. Liu, W. Fu, N.J. Dudney, and C. Liang, *Angew. Chem. Int. Ed.* **52**, 7460 (2013).
25. R.S.C. Smart, W.M. Skinner and A.R. Gerson, *Surf. Interface Anal.* **28**, 101 (1999).
26. M. Fantauzzi, B. Elsener, D. Atzei, A. Rigoldi and A. Rossi, *RSC Adv.* **5**, 75953 (2015).
27. H. Muramatsu, A. Hayashi, T. Ohtomo, S. Hama and M. Tatsumisago, *Solid State Ionics* **182**, 116 (2011).
28. G. Sahu, Z. Lin, J. Li, Z. Liu, N.J. Dudney and C. Liang, *Energy Environ. Sci.* **7**, 1053 (2014).